Constant Power Control and Fault-Ride-Through Enhancement of DFIG Wind Turbines with Energy Storage

Liyan Qu
Ansoft, LLC
Irvine, CA 92602 USA
liyanqu@ieee.org

Wei Qiao
Department of Electrical Engineering
University of Nebraska−Lincoln
223N Walter Scott Engineering Center
Lincoln, NE 68588-0511 USA
wqiao@engr.unl.edu

***Abstract*—With the increasing penetration of wind power into electric power grids, energy storage devices will be required to dynamically match the intermittency of wind energy. This paper proposes a novel two-layer constant-power control scheme for a wind farm equipped with doubly-fed induction generator (DFIG) wind turbines. Each DFIG wind turbine is equipped with a supercapacitor energy storage system (ESS) and is controlled by the low-layer WTG controllers and coordinated by a high-layer wind-farm supervisory controller (WFSC). The WFSC generates the active-power references for the low-layer WTG controllers according to the active-power demand from the grid operator; the low-layer WTG controllers then regulate each DFIG wind turbine to generate the desired amount of active power, where the deviations between the available wind energy input and desired active power output are compensated by the ESS. Simulation studies are carried out in PSCAD/EMTDC on a wind farm equipped with 15 DFIG wind turbines to verify the effectiveness of the proposed control scheme.**

Keywords-constant-power control (CPC); doubly-fed induction generator (DFIG); energy storage; supervisory controller; wind turbine

I. INTRODUCTION

Wind turbine generators (WTGs) are usually controlled to generate maximum electrical power from wind under normal wind conditions. However, because of the variations of wind speed, the generated electrical power of a WTG is usually fluctuated. Currently, wind energy only provides about 1%–2% of the U.S.'s electricity supply. At such a penetration level, it is not necessary to require WTGs to participate in grid frequency regulation, unit commitment, or to supply a constant amount of active power as required by the grid operator.

However, it is reasonable to expect that wind power will be capable of becoming a major contributor to the nation's and world's electricity supply over the next three decades. For instance, the European Wind Energy Association (EWEA) has set a target to satisfy more than 22% of European electricity demand with wind power by 2030 [1]. In the U.S., according to a report [2] by the Department of Energy, it is feasible to supply 20% of the nation's electricity from wind by 2030. At such high levels of penetration, it will become necessary to require WTGs to participate in grid frequency regulation as well as to supply the desired amount of active power for power flow control [3].

To meet the requirements of frequency and active power regulation, energy storage devices will be required to dynamically match the intermittency of wind energy. In [4], the authors investigated and compared different feasible electrical energy storage technologies for intermittent renewable energy generation, such as wind power. The use of supercapacitors [5] or batteries [6]-[8] as energy storage devices for WTGs has been studied by some researchers. However, these studies only focused on control and operation of individual WTGs and did not investigate the issues of WTGs to participate in grid regulation.

This paper proposes a novel two-layer constant-power control (CPC) scheme for a wind farm equipped with doubly-fed induction generator (DFIG) wind turbines, where each WTG is equipped with a supercapacitor energy storage system (ESS). The CPC consists of a high-layer wind-farm supervisory controller (WFSC) and multiple low-layer WTG controllers. The high-layer WFSC generates the active-power references for the low-layer WTG controllers of each individual DFIG wind turbine according to the active-power demand from the grid operator. The low-layer WTG controllers then regulate each DFIG wind turbine to generate the desired amount of active power, where the deviations between the available wind energy input and desired active power output are compensated by the ESS. Simulation studies are carried out in PSCAD/EMTDC on a wind farm equipped with 15 DFIG wind turbines to verify the effectiveness of the proposed control scheme.

II. DFIG WIND TURBINE WITH ENERGY STORAGE

Fig. 1 shows the basic configuration of a DFIG wind turbine equipped with a supercapacitor-based ESS. The low-speed wind turbine drives a high-speed DFIG through a gearbox. The DFIG is a wound-rotor induction machine. It is connected to the power grid at both stator and rotor terminals. The stator is directly connected to the grid while the rotor is fed through a variable-frequency dc-link-voltage converter, which consists of a rotor-side converter (RSC) and a grid-side converter (GSC) and usually has a rating of a fraction (25%–

This work was supported in part by the UNL Research Council Faculty Seed Grant.

978-1-4244-3476-3/09/$25.00 ©2009 IEEE

30%) of the DFIG nominal power. As a consequence, the WTG can operate with the rotational speed in a range of ±25%–30% around the synchronous speed, and its active and reactive powers can be controlled independently.

In this work, an ESS consisting of a supercapacitor bank and a two-quadrant dc/dc converter is connected to the dc link of the DFIG converters. The ESS serves as either a source or a sink of active power, and therefore, contributes to control the generated active power of the WTG.

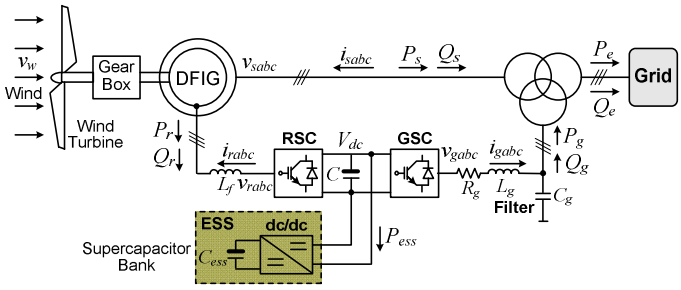

Fig. 1. Configuration of a DFIG wind turbine equipped with a supercapacitor ESS connected to a power grid.

III. Wind Farm Model

Fig. 2 shows the configuration of the wind farm used in this work. It consists of 15 DFIG wind turbines of 3.6 MW power capacity each [9]-[10]. The total power capacity of the wind farm is 54 MW. Each DFIG wind turbine (see Fig. 1) is connected to the internal network of the wind farm through a 4.16/34.5-kV voltage step-up transformer. The high-voltage terminals of all transformers in the wind farm are connected by 34.5-kV power cables to form the internal network of the wind farm. The entire wind farm is connected to the utility power grid through a 34.5/138-kV voltage step-up transformer at the point of common coupling (PCC) to supply active and reactive powers of P and Q, respectively. In this work, the power grid is represented by an infinite source.

IV. Control Of Individual DFIG Wind Turbine

The control system of each individual DFIG wind turbine generally consists of two parts: the electrical control of the DFIG and the mechanical control of the wind turbine blade pitch angle [9]. Control of the DFIG is achieved by controlling the RSC, the GSC, and the ESS (see Fig. 1). The control objective of the RSC is to regulate the stator-side active power P_s and reactive power Q_s independently. The control objective of the GSC is to maintain the dc-link voltage V_{dc} constant and to regulate the reactive power Q_g that the GSC exchanges with the grid. The control objective of the ESS is to regulate the active power P_g that the GSC exchanges with the grid.

A. Control of the RSC

Fig. 3 shows the overall vector control scheme of the RSC, in which the independent control of the stator active power P_s and reactive power Q_s is achieved by means of rotor current regulation in a stator-flux oriented synchronously rotating reference frame [11]. Therefore, the overall RSC control

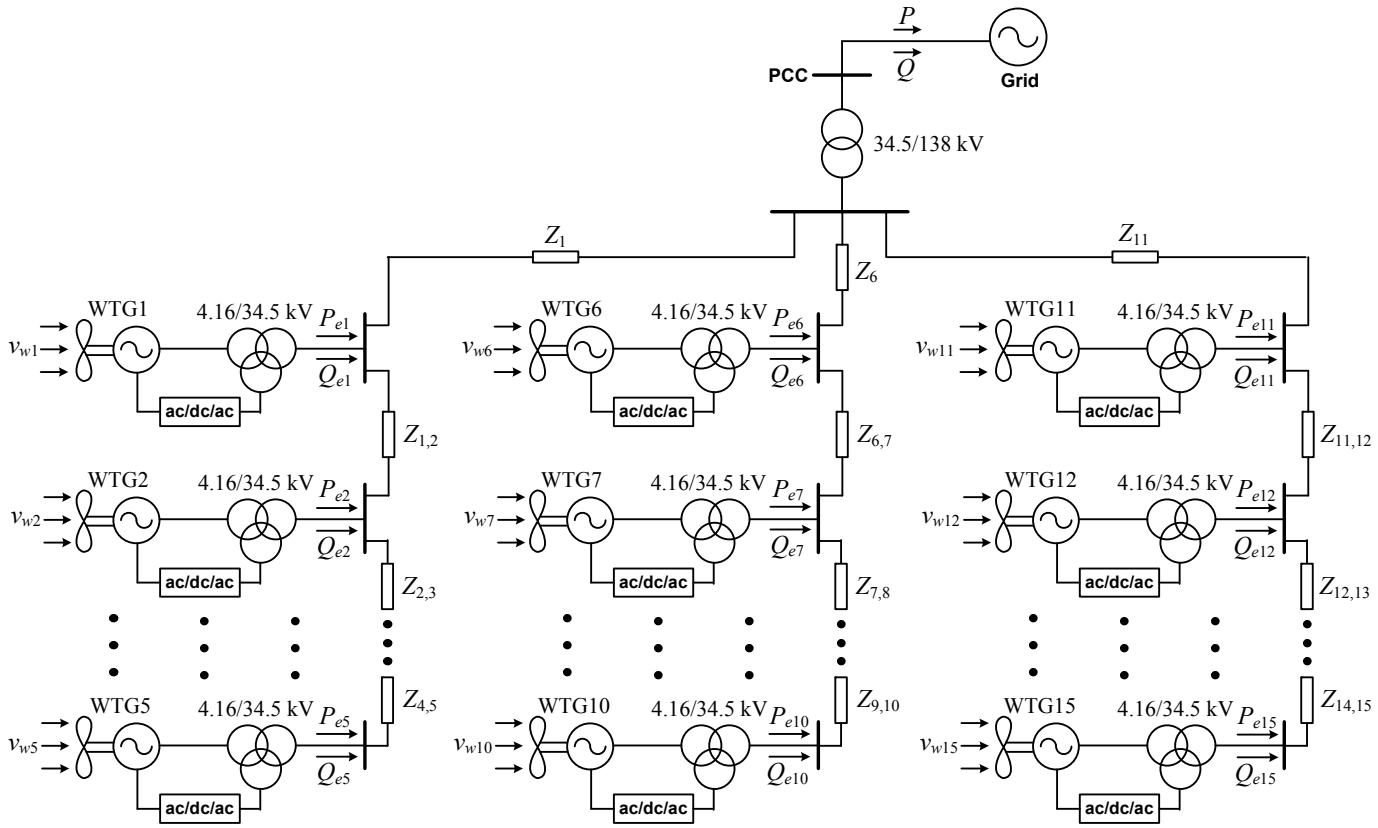

Fig. 2. Configuration of a wind farm equipped with 15 DFIG wind turbines connected to a power grid.

scheme consists of two cascaded control loops. The outer control loop regulates the stator active and reactive powers independently, which generates the reference signals i_{dr}^* and i_{qr}^* of the *d*-axis and *q*-axis current components, respectively, for the inner-loop current regulation. The outputs of the two current controllers are compensated by the corresponding cross-coupling terms v_{dr0} and v_{qr0} [9], respectively, to form the total voltage signals, v_{dr} and v_{qr}. They are then used by the PWM module to generate the gate control signals to drive the RSC. The reference signals of the outer-loop power controllers are generated by the high-layer WFSC.

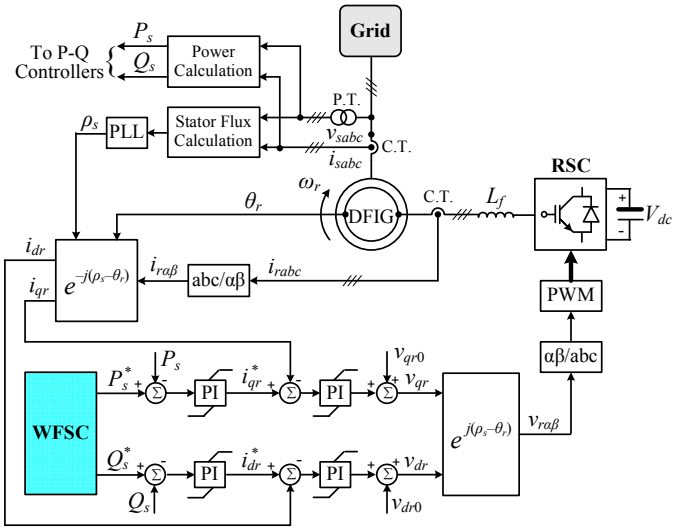

Fig. 3. Overall vector control scheme of the RSC.

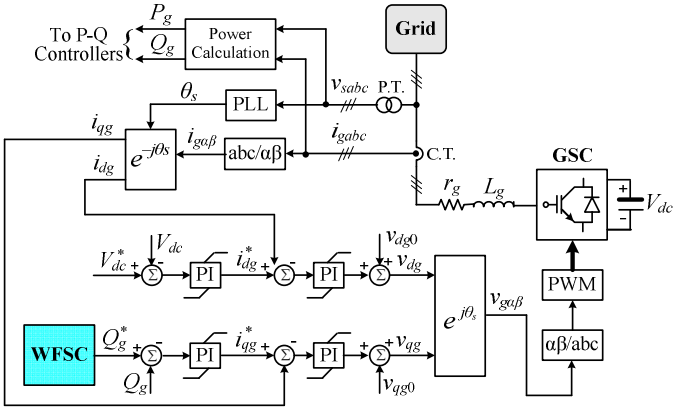

Fig. 4. Overall vector control scheme of the GSC.

B. Control of the GSC

Fig. 4 shows the overall vector control scheme of the GSC, in which the control of the dc-link voltage V_{dc} and the reactive power Q_g exchanged between the GSC and the grid is achieved by means of current regulation in a synchronously rotating reference frame [11]. Again, the overall GSC control scheme consists of two cascaded control loops. The outer control loop regulates the dc-link voltage V_{dc} and the reactive power Q_g, respectively, which generates the reference signals i_{dg}^* and i_{qg}^* of the *d*-axis and *q*-axis current components, respectively, for the inner-loop current regulation. The outputs of the two current controllers are compensated by the corresponding cross-coupling terms v_{dg0} and v_{qg0} [9], respectively, to form the total voltage signals, v_{dg} and v_{qg}. They are then used by the PWM module to generate the gate control signals to drive the GSC. The reference signal of the outer-loop reactive-power controller is generated by the high-layer WFSC.

C. Conficuration and Control of the ESS

Fig. 5 illustrates the configuration and control of the ESS. The ESS consists of a supercapacitor bank and a two-quadrant dc/dc converter connected to the dc link of the DFIG. The dc/dc converter contains two IGBT switches S_1 and S_2. Their duty ratios are controlled to regulate the active power P_g that the GSC exchanges with the grid. In this configuration, the dc/dc converter can operate in two different modes, i.e., buck or boost mode, depending on the status of the two IGBT switches. If S_1 is closed and S_2 is open, the dc/dc converter operates in the buck mode; if S_1 is open and S_2 is closed, the dc/dc converter operates in the boost mode. The duty ratio D_1 of S_1 can be approximately expressed as

$$D_1 = \frac{V_{SC}}{V_{dc}} \tag{1}$$

and the duty ratio D_2 of S_2 is $D_2 = 1 - D_1$. In this paper, the nominal dc-voltage ratio $V_{SC,n}/V_{dc,n}$ is 0.5, where $V_{SC,n}$ and $V_{dc,n}$ are the nominal voltages of the supercapacitor bank and the DFIG dc link, respectively. Therefore, the nominal duty ratio $D_{1,n}$ of S_1 is 0.5.

The duty ratio D_1 of the dc/dc converter is controlled depending on the relationship between the active powers P_r of the RSC and P_g of the GSC. If P_r is greater than P_g, D_1 is controlled greater than 0.5. Consequently, the supercapacitor bank serves as a sink to absorb active power, which results in the increase of its voltage V_{SC}. On the contrary, if P_g is greater than P_r, D_1 is controlled less than 0.5. Consequently, the supercapacitor bank serves as a source to supply active power, which results in the decrease of its voltage V_{SC}. Therefore, by controlling the duty ratio of the dc/dc converter, the ESS serves as either a source or a sink of active power to control the generated active power of the WTG. In Fig. 5, the reference signal P_g^* is generated by the high-layer WFSC.

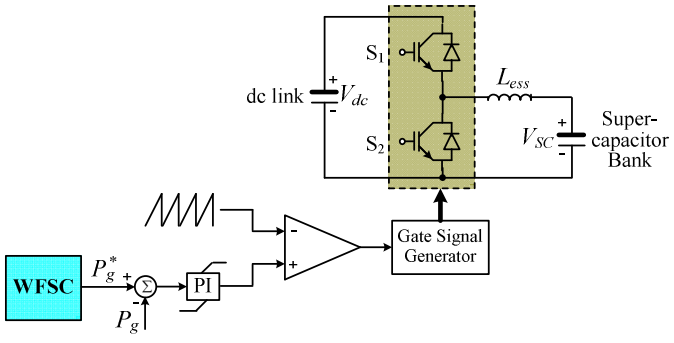

Fig. 5. Configuration and control of the ESS.

V. WIND-FARM SUPERVISORY CONTROL

The objective of the WFSC is to generate the reference singles for the outer-loop power controllers of the RSC and GSC as well as the controller of the dc/dc converter of each WTG, according to the power demands from the grid operator. The implementation of the WFSC is described by the flow chart in Fig. 6, where P_d is the active power demand from the grid operator; v_{wi} and V_{essi} are the wind speed in m/s and the voltage of the supercapacitor bank measured from WTG i (i = 1, ···, 15). Based on v_{wi}, the optimal rotational speed $\omega_{ti,opt}$ in rad/s of the wind turbine can be determined, which is proportional to the wind speed v_{wi} at a certain pitch angle β_i:

$$\omega_{ti,opt} = k(\beta_i)\, v_{wi} \tag{2}$$

where k is a constant at a certain value of β_i. Then, the maximum mechanical power $P_{mi,max}$ that the wind turbine extracts from the wind can be calculated by the well-known wind-turbine aerodynamic characteristics:

$$P_{mi,\max} = \frac{1}{2}\rho_i A_r v_{wi}^3 C_{Pi}(\lambda_{i,opt}, \beta_i) \tag{3}$$

where ρ_i is the air density in kg/m^3; $A_r = \pi R^2$ is the area in m^2 swept by the rotor blades and R is the blade length in m; C_{Pi} is the power coefficient, which is a function of both tip-speed-ratio λ_i and the blade pitch angle β_i, where λ_i is defined by:

$$\lambda_i = \frac{\omega_{ti} R}{v_{wi}} \tag{4}$$

In (3) $\lambda_{i,opt}$ is the optimal tip-speed-ratio when the wind turbine rotates with the optimal speed $\omega_{ti,opt}$ at the wind speed v_{wi}.

Given $P_{mi,max}$, the maximum active power $P_{ei,max}$ generated by the WTG can be estimated by taking into account the power losses of the WTG [9].

$$P_{ei,max} = P_{mi,max} - P_{Li} = P_{si,max} + P_{ri,max} \tag{5}$$

where P_{Li} is the total power losses of WTG i, which can be estimated by the method in [9]; $P_{si,max}$ and $P_{ri,max}$ are the maximum DFIG stator and rotor active powers of WTG i, respectively. In terms of the instantaneous variables in Fig. 1, the stator active power P_s can be written in a synchronously rotating d-q reference frame [11] as follows.

$$P_s = \frac{3}{2}(v_{ds} i_{ds} + v_{qs} i_{qs}) \approx \frac{3}{2}[\omega_s L_m (i_{qs} i_{dr} - i_{ds} i_{qr}) + r_s (i_{ds}^2 + i_{qs}^2)] \tag{6}$$

where v_{ds} and v_{qs} are the d-axis and q-axis voltage components of the stator windings, respectively; i_{ds} and i_{qs} are the stator d-axis and q-axis current components, respectively; i_{dr} and i_{qr} are the rotor d-axis and q-axis current components, respectively; ω_s is the rotational speed of the synchronous reference frame; r_s and L_m are the stator resistance and mutual inductance, respectively. Similarly, the rotor active power is calculated by:

$$P_r = \frac{3}{2}(v_{dr} i_{dr} + v_{qr} i_{qr}) \approx \frac{3}{2}[-s\omega_s L_m (i_{qs} i_{dr} - i_{ds} i_{qr}) + r_r (i_{dr}^2 + i_{qr}^2)] \tag{7}$$

where v_{dr} and v_{qr} are the d-axis and q-axis voltage components of the rotor windings, respectively; s is the slip of the DFIG defined by:

$$s = (\omega_s - \omega_r)/\omega_s \tag{8}$$

where ω_r is the DFIG rotor speed. Equations (6) and (7) yield

$$s = -\frac{P_r - 3i_r^2 r_r}{P_s - 3i_s^2 r_s} \tag{9}$$

where $i_s = \sqrt{i_{ds}^2 + i_{qs}^2}/2$ and $i_r = \sqrt{i_{dr}^2 + i_{qr}^2}/2$. If neglecting the stator copper loss $3i_s^2 r_s$ and rotor copper loss $3i_r^2 r_r$ of the DFIG, the relationship between the stator and rotor active powers can be approximated by

$$P_r = -sP_s \tag{10}$$

According to (5) and (9) [or (10)], $P_{si,max}$ and $P_{ri,max}$ of each WTG can be determined. Then, the total maximum mechanical power $P_{m,max}$, DFIG output active power $P_{e,max}$, and stator active power $P_{s,max}$ of all WTGs in the wind farm can be calculated.

$$P_{m,\max} = \sum_{i=1}^{15} P_{mi,\max} \tag{11}$$

$$P_{e,\max} = \sum_{i=1}^{15} P_{ei,\max} \tag{12}$$

$$P_{s,\max} = \sum_{i=1}^{15} P_{si,\max} \tag{13}$$

In order to supply constant power P_d to the grid, the deviation (called $P_{ess,d}$) between the demand P_d and the maximum generation $P_{e,max}$ is the power that should be stored in or supplied from the ESSs of the WTGs.

$$P_{ess,d} = P_{e,max} - P_d \tag{14}$$

On the other hand, the capability of each ESS to store or supply power depends on the capacitance C_{ess} and the voltage V_{essi} of the supercapacitor bank. During normal operation, V_{essi} must be maintained within the following range:

$$V_{i,min} < V_{essi} < V_{i,max} \tag{15}$$

where $V_{i,max}$ and $V_{i,min}$ are the maximum and minimum operating voltages of the supercapacitor bank, respectively. The maximum power $P_{essi,max}$ that can be exchanged between the supercapacitor bank and the DFIG dc link of WTG i can be determined by:

$$P_{essi,\max} = \pm C_{ess} V_{essi} \left| \frac{dV_{essi}}{dt} \right|_{\max} \tag{16}$$

where $|dV_{essi}/dt|_{max}$ is the maximum rate of voltage variations of the supercapacitor bank, which is related to the current limits of the supercapacitor bank. In (16), the positive sign indicates storing energy while the negative sign indicates supplying energy by the ESS, respectively. The calculation of $P_{essi,max}$ for each WTG is subjected to (15). Fig. 7 illustrates how to determine $P_{essi,max}$ for each WTG. If $P_{ess,d} > 0$, extra power needs to be stored in the ESSs. In this case, if $V_{essi} < V_{i,max}$, $P_{essi,max}$ is calculated by (16) and takes the positive sign; otherwise, the ESS cannot store any power and $P_{essi,max} = 0$. On the contrary, if $P_{ess,d} < 0$, active power needs to be supplied

from the ESSs. In this case, if $V_{essi} > V_{i,min}$, $P_{essi,max}$ is calculated by (16) and takes the negative sign; otherwise, the ESS cannot supply any power and $P_{essi,max} = 0$.

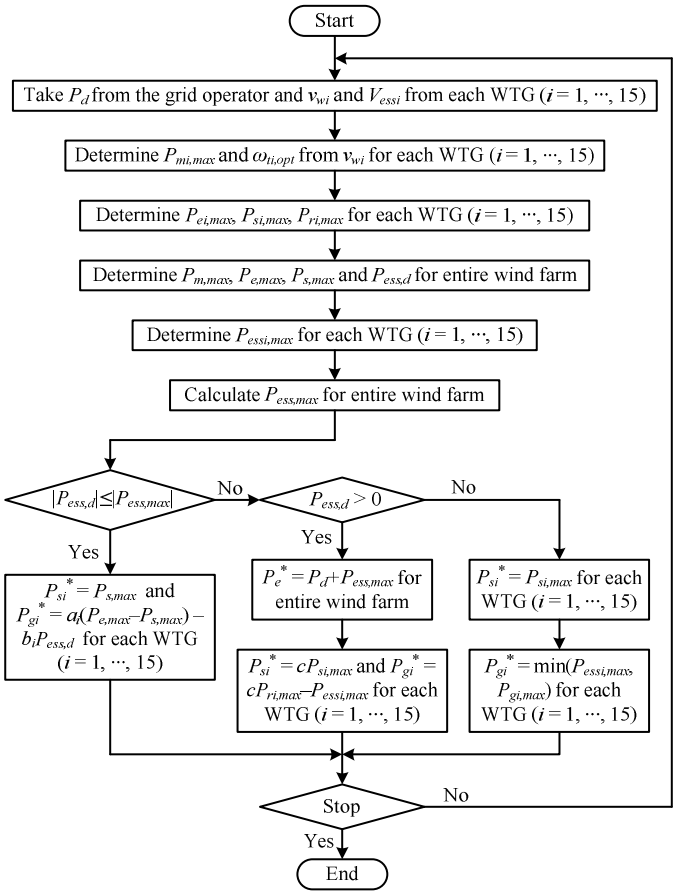

Fig. 6. Flow chart for implementation of the WFSC.

As shown in Fig. 6, once $P_{essi,max}$ of each WTG is determined, the total maximum power $P_{ess,max}$ that can be exchanged between the supercapacitor bank and the DFIG dc link of all WTGs can be determined by:

$$P_{ess,\max} = \sum_{i=1}^{15} P_{essi,\max} \tag{17}$$

Finally, depending on the relationship of $P_{ess,d}$ and $P_{ess,max}$, the reference signals P_{si}^* (see Fig. 3) and P_{gi}^* (see Fig. 5) of each WTG can be determined. Specifically, if $|P_{ess,d}| \le |P_{ess,max}|$, P_{si}^* and P_{gi}^* can be determined directly, as shown in Fig. 6, where the partition coefficients a_is are calculated by:

$$a_i = \frac{P_{ri,\max}}{P_{e,\max} - P_{s,\max}} \tag{18}$$

and the partition coefficients b_is are calculated by:

$$b_i = \frac{P_{essi,\max}}{P_{ess,d}} \tag{19}$$

The coefficients a_i and b_i have the following feature:

$$\sum_{i=1}^{15} a_i = 1 \text{ and } \sum_{i=1}^{15} b_i = 1 \tag{20}$$

If $|P_{ess,d}| > |P_{ess,max}|$, depending on the sign of $P_{ess,d}$, P_{si}^* and P_{gi}^* can be determined respectively, as shown in Fig. 6. If $P_{ess,d}$ is positive, the ESSs of all WTGs store active power; and the total active power generated by all DFIGs is P_e^*, which is less than $P_{e,max}$. Therefore, a scaling factor c is defined as follows:

$$c = \frac{P_e^*}{P_{e,\max}} \tag{21}$$

and P_{si}^* and P_{gi}^* can be determined by using the scaling factor. If $P_{ess,d}$ is negative, the ESSs of all WTGs supply active power; the RSC of each WTG is controlled to generate the maximum stator active power $P_{si,max}$; and the ESS of each WTG is controlled to generate active power of P_{gi}^*, where $P_{gi,max}$ is the maximum value of P_{gi} depending on the maximum power capacity of the GSC.

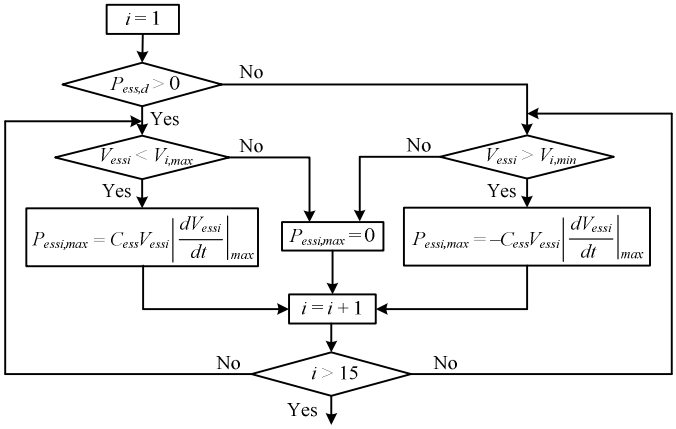

Fig. 7. Flow chart for determination of $P_{essi,max}$ for each WTG.

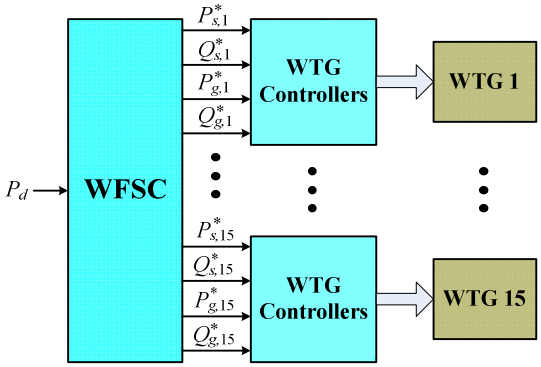

Fig. 8. Proposed two-layer CPC scheme for the wind farm.

The reactive power references of the RSC (Fig. 3) and GSC (Fig. 4) controllers can be determined by controlling the power factor at the PCC at the desired value, which is not in the scope of this paper. In this work, the reactive power references of all RSC and GSC controllers are simply set as zero.

Fig. 8 shows the block diagram of the proposed two-layer CPC scheme for the wind farm, where P_d is the active power demand from the grid operator. In practice, the value of P_d should take into account the power-generation capability of the wind farm and should be subjected to the following limits.

$$P_d \le \overline{P}_{e,\max} \tag{22}$$

where $\overline{P}_{e,\max}$ is the average maximum active power (i.e., the average value of $P_{e,max}$ over time) that can be generated by the wind farm during the period that P_d is constant.

VI. Simulation Results

Simulation studies are carried out to verify the effectiveness of the proposed control scheme under various operating conditions. Some typical results are shown and discussed in this section.

A. Constant Power Control during Variable Wind-Speed Conditions

Fig. 9 shows the wind speed profiles applied to WTG1 (v_{w1}), WTG6 (v_{w6}), and WTG11 (v_{w11}). The wind speeds across the three WTGs vary in a range of ±3 m/s around their mean value of 12 m/s. The variations of wind speed cause fluctuations of the electrical quantities of the WTGs. As shown in Fig. 10, if the wind farm is not equipped with any energy storage devices or the proposed CPC scheme, the wind-speed variations in the wind farm result in the significant fluctuations of the total output active power at the PCC. The wind-farm power output deviates significantly from the active-power demand of the grid operator. In future electric power grids where the penetration of wind power is high (e.g., 20%), such active power fluctuations can bring severe problems to grid operation.

Fig. 11 compares the total output active power of the wind farm with the power demand from the grid operator, where each WTG is equipped with an ESS as shown in Fig. 1. The ESS stores energy when the WTG generates more active power than the demand and supplies energy when the WTG generates less active power than the demand. The resulting output power of the wind farm is therefore controlled at a constant value as required by the grid operator.

Fig. 12 shows the total stator active power P_s and the total GSC active power P_g of all WTGs, as well as the total output active power P (measured at PCC) of the wind farm. Through the control of the proposed CPC scheme, the variations of the stator active power are exactly compensated by the variations of the GSC active power. Consequently, the total output active power of the wind farm is constant. However, the total output active power P_{ei} of each individual WTG, which is the sum of the stator active power P_{si} and the GSC active power P_{gi}, is usually not constant, as shown in Fig. 13. The deviations between the RSC active power and the GSC active power of each WTG are stored in or supplied by the ESS.

Fig. 14 shows the voltages of the supercapacitor banks of WTG1, WTG6, and WTG11. These voltages are always maintained within the operating limits of [0.7, 1.1] p.u.

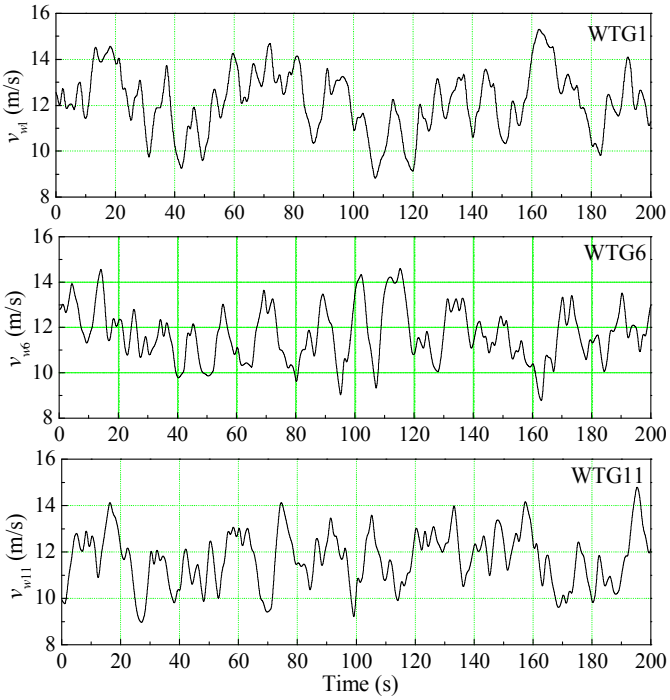

Fig. 9. Wind speed profiles of WTG1, WTG6, and WTG11.

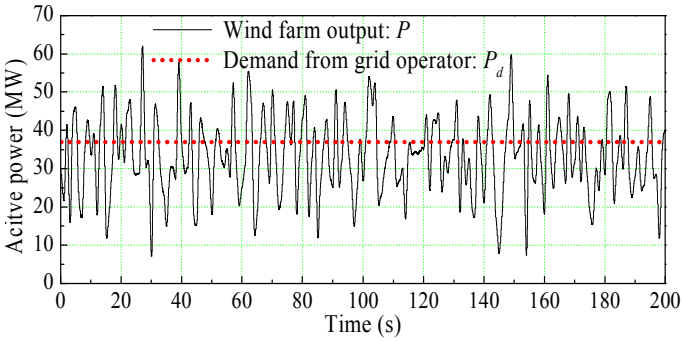

Fig. 10. Comparison of the wind-farm output power (measured at PCC) and the constant power demand from the grid operator: without ESSs and the proposed CPC scheme.

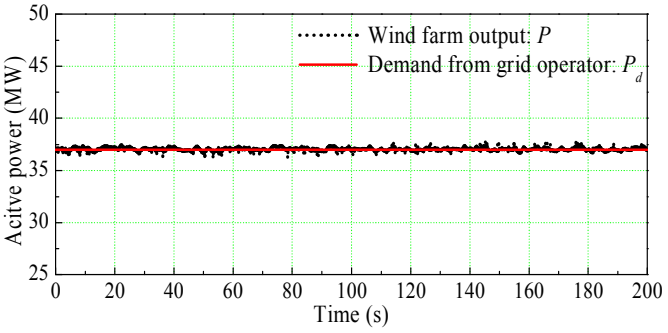

Fig. 11. Comparison of the wind-farm output power (measured at PCC) and the constant power demand from the grid operator: with ESSs and the proposed CPC scheme.

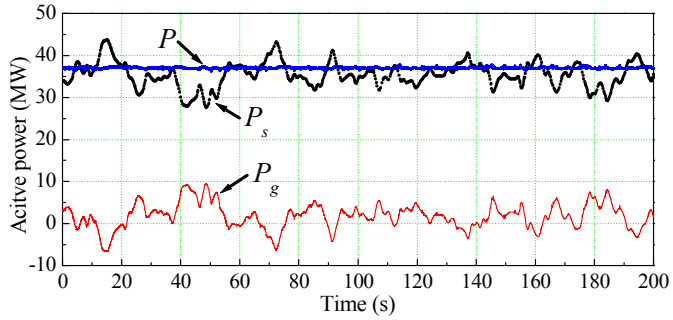

Fig. 12. Active powers of all WTGs and the wind farm.

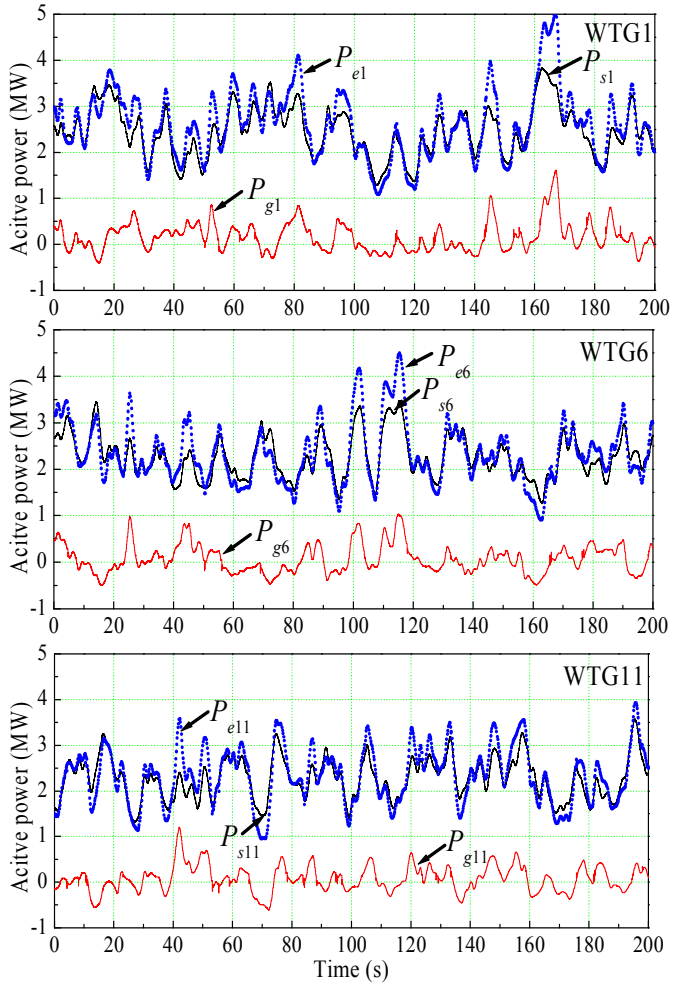

Fig. 13. Active powers of individual WTGs.

B. *Power Tracking during Step Changes in Demand*

Under the same wind conditions as in the previous tests, the power demand from the grid operator is now step changed from time to time. The wind farm is controlled by the proposed CPC scheme to track the variations of the power demand. Fig. 15 shows the power tracking performance of the wind farm. The generated active power by the wind farm dynamically tracks the power demand with good precision. This power tracking capability cannot be achieved without using the ESSs or the proposed control scheme.

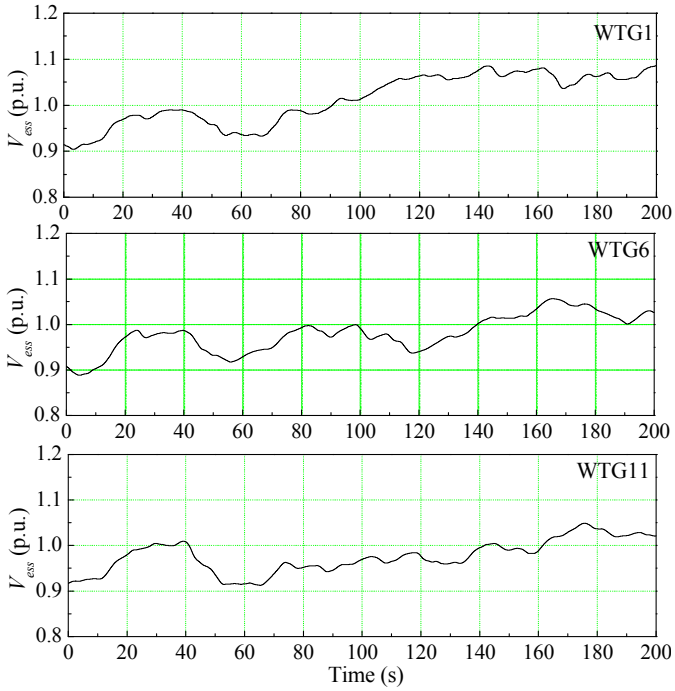

Fig. 14. Voltages of the supercapacitor banks of WTG1, WTG6, and WTG11.

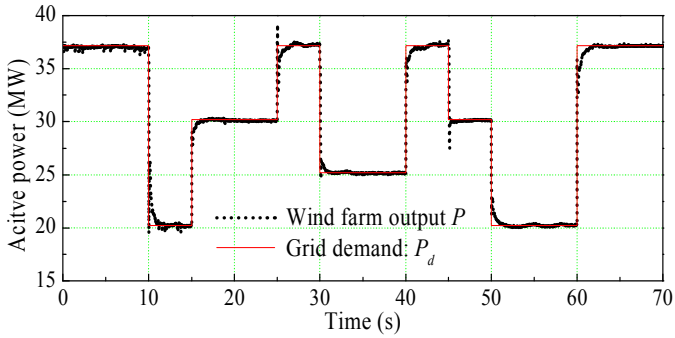

Fig. 15. Power tracking performance of the wind farm during step changes in demand from the grid operator.

In addition, by using the ESSs as the source or sink of active power, it is possible to control the power imbalance or power oscillations during grid fault conditions, therefore enhancing the fault-ride-through capability of the wind farm. This issue will be investigated in future work.

VII. Conclusion

This paper has proposed a novel two-layer CPC scheme for a wind farm equipped with DFIG wind turbines. Each wind turbine is equipped with a supercapacitor-based ESS, which is connected to the dc link of the DFIG. The ESS and the controllers of each individual DFIG wind turbine have been suitably designed. A high-layer WFSC has been developed to coordinate the actions of the low-layer individual WTG controllers. Consequently, the wind farm generates constant active power as required by the grid operator. Simulation studies have been carried out on a wind farm equipped with 15

DFIG wind turbines to verify the effectiveness of the proposed CPC scheme. Results have shown that the proposed CPC scheme enabled the wind farm to actively participate in active power regulation of the grid. The proposed system and control scheme provides a promising solution to help achieve high levels of penetration of wind power into electric power grids.

VIII. Appendix

Wind turbine (Fig. 1): rated capacity = 3.6 MW, number of blades = 3, rotor diameter = 104 m, swept area = 8495 m^2, rotor speed (variable) = 8.5-15.3 rpm.

Wound-rotor induction generator (Fig. 1): nominal power = 3.6 MW, nominal stator voltage = 4.16 kV, power factor pf = –0.9 ~ +0.9, r_s = 0.0079 p.u., r_r = 0.025 p.u., r_m = 66.57 p.u., L_{ls} = 0.07937 p.u., L_{lr} = 0.40 p.u., L_m = 4.4 p.u., base frequency f = 60 Hz.

ESS (Figs. 1 and 5): C = 20 mF, C_{ess} = 20 F, L_{ess} = 50 mH, nominal dc-link voltage = 4 kV, nominal voltage of the supercapacitor bank = 2 kV.

Power network (Fig. 2): Each power cable is represented by a Π equivalent circuit where $Z_1 = Z_6 = Z_{11}$ = 0.0738+j0.1050 Ω and the shunt admittance is $-jB_1/2 = -j2.6901\times10^{-5}$ S; $Z_{1,2} = Z_{6,7} = Z_{11,12}$ = 0.0771+j0.1148 Ω and the shunt admittance is $-jB_2/2 = -j2.2263\times10^{-5}$ S; $Z_{2,3} = Z_{7,8} = Z_{12,13}$ = 0.1870+j0.1444 Ω and the shunt admittance is $-jB_3/2 = -j1.6388\times10^{-5}$ S; $Z_{3,4} = Z_{8,9} = Z_{13,14}$ = 0.2756+j0.1558 Ω and the shunt admittance is $-jB_4/2 = -j1.4842\times10^{-5}$ S; $Z_{4,5} = Z_{9,10} = Z_{14,15}$ = 0.3658+j0.1591 Ω and the shunt admittance is $-jB_4/2 = -j1.3296\times10^{-5}$ S. The shunt admittances are not drawn in Fig. 2.

References

[1] "Focus on 2030: EWEA aims for 22% of Europe's electricity by 2030," *Wind Directions*, pp. 25-34, Nov./Dec. 2006.

[2] "20% wind energy by 2030: increasing wind energy's contribution to U.S. electricity supply," U.S. Department of Energy, July 2008.

[3] W. Qiao and R. G. Harley, "Grid connection requirements and solutions for DFIG wind turbines," in *Proc. IEEE Energy 2030 Conference*, Atlanta, GA, USA, Nov. 17-18, 2008.

[4] J. P. Barton and D. G. Infield, "Energy storage and its use with intermittent renewable energy," *IEEE Trans. Energy Conversion*, vol. 19, no. 2, pp. 441-448, June 2004.

[5] C. Abbey and G. Joos, "Supercapacitor energy storage for wind energy applications," *IEEE Trans. Industry Applications*, vol. 43, no. 3, 769-776, May/June 2007.

[6] B. S. Borowy and Z. M. Salameh, "Dynamic response of a stand-alone wind energy conversion system with battery energy storage to wind gust," *IEEE Trans. Energy Conversion*, vol. 12, no. 1, pp. 73-78, Mar. 1997.

[7] M.-S. Lu, C.-L. Chang, W.-J. Lee, and L. Wang, "Combining the wind power generation system with energy storage equipments," in *Proc. IEEE IAS 43rd Annual Meeting*, Edmonton, Canada, October 5-9, 2008.

[8] A. Yazdani, "Islanded operation of a doubly-fed induction generator (DFIG) wind-power system with integrated energy storage," in *Proc. 2007 IEEE Canada Electrical Power Conference*, Montreal, Quebec, Oct. 25-26, 2007, pp. 153-159.

[9] W. Qiao, W. Zhou, J. M. Aller, and R. G. Harley, "Wind speed estimation based sensorless output maximization control for a wind turbine driving a DFIG," *IEEE Trans. Power Electronics*, vol. 23, no. 3, pp. 1156-1169, May 2008.

[10] W. Qiao, G. K. Venayagamoorthy, and R. G. Harley, "Real-time implementation of a STATCOM on a wind farm equipped with doubly fed induction generators," *IEEE Trans. Industry Applications*, vol. 45, no. 1, pp. 98-107, Jan./Feb. 2009.

[11] D. W. Novotny and T. A. Lipo, *Vector Control and Dynamics of AC Drives*, Oxford University Press, 2000.